ISSN 0469-4732

INSTITUTE OF PLASMA PHYSICS

NAGOYA UNIVERSITY

Simulation of Tokamak Runaway-Electron Events – Study of the Response of Materials by Use of an Electron Linear Accelerator

H. Bolt, A. Miyahara, M. Miyake, T. Yamamoto

(Received – July 17, 1987)

IPPJ- 841 Aug. 1987

RESEARCH REPORT

NAGOYA, JAPAN

Simulation of Tokamak Runaway-Electron Events - Study of the Response of Materials by Use of an Electron Linear Accelerator

H. Bolt[1], A. Miyahara[2], M. Miyake[3], T. Yamamoto[4]

[1] Inst. of Plasma Physics, Nagoya University; on leave from Inst. for Reactor Materials, Kernforschungsanlage Juelich GmbH, FRG, Assoziation EURATOM - KFA

[2] Inst. of Plasma Physics, Nagoya University

[3] Dept. of Nuclear Engineering, Osaka University

[4] Inst. of Scientific and Industrial Research, Osaka University

Abstract:

High energy runaway-electron events which can occur in tokamaks when the plasma hits the first wall are a critical issue for the materials selection of future devices. Runaway-electron events are simulated with an electron linear accelerator to better understand the observed runaway-electron damage to tokamak first wall materials and to consider the runaway-electron issue in further materials development and selection. The electron linear accelerator produces beam energies of 20 to 30 MeV at an integrated power input of up to 1.3 kW. Graphite, SiC + 2%AlN, stainless steel, molybdenum and tungsten have been tested as bulk materials. To test the reliability of actively cooled systems under runaway-electron impact layer systems of graphite fixed to metal substrates have been tested. The irradiation resulted in damage to the metal compounds but left graphite and SiC + 2%AlN without damage. Metal substrates of graphite - metal systems for actively cooled structures suffer severe damage unless thick graphite shielding is provided.

1. Introduction

Disrupting plasmas and low density edge plasmas have been observed to produce electrons which are accelerated to high energies /1,2/. Since the electron scattering cross section in hydrogen plasmas decreases significantly at relativistic energies, this enables further acceleration leading to the runaway-electron phenomenon. In present tokamaks the energy spectrum of runaway-electrons ranges from a few MeV in medium size tokamaks to more than 30 MeV in large size devices /2,3,4/. During positional instabilities of the plasma, particularly in the course of disruptions, these electrons may intersect with components of the first wall. Runaway-electron interaction times with wall components are reported to be 20 to 40 ms in the case of JET /4/.The stopping process of runaway-electrons in first wall materials is determined by the electron energy and the physical properties of the materials and may lead to volume heating, photon and neutron production. The deposition of the electron kinetic energy in these components may lead to severe damage like melting, evaporation and cracking /2,3/.

A program of runaway-electron simulation experiments by use of an electron linear accelerator was developed to clarify the wall side processes under runaway-electron impact. Bulk materials covering a broad range in atomic number Z and density ρ and layer compound systems of low density, low Z materials covering high density, high Z metal substrates were studied. Special attention was paid to such material compound systems since they are expected to be increasingly applied as actively cooled first wall structures with metal cooling tubes covered by low Z

materials (e.g. graphite brazed to molybdenum in ASDEX-upgrade) /5/. It is anticipated that runaway-electrons might easily pass the low density layer of these systems and deposit the major part of their energy in the metal cooling tubes thus leading to excessive heating and possibly to failure of these structures.

2. Experimental procedure

Experiments were carried out with the electron linear accelerator of the Institute of Scientific and Industrial Research of Osaka University. The experimental parameters are given in Table 1.
After preliminary experiments under atmosphere a vacuum chamber was constructed to prevent beam spread and excessive oxidation of the specimen surfaces. The experimental set-up is shown in Figure 1. Most experiments were carried out under a vacuum of 10^{-1} Torr. After being coupled out of the linac tube guide by a 20 µm thick Ti-window the electron beam is passed directly into the target chamber through the same kind of 20 µm Ti-window. The linac tube guide and the experimental chamber had to be separated from each other to prevent contamination of the electron beam facility. The specimen surfaces subjected to normal beam incidence were polished before the experiments.

After the decay of induced activity, post experimental examinations were carried out to determine damage caused by high energy electron impact. This included visual examination, metallography, optical light microscopy and SEM observations.

3. Experimental results

3.1 Experimental results on bulk materials

Bulk materials covering a wide range of densities were chosen for the experiments. The materials tested, their relevant physical properties and specimen geometry are listed in Table 2.
The experimental results depending on the experimental conditions are given in Table 3 in the form of damage thresholds.

The irradiation of graphite with 20 to 30 MeV at times of up to 60 s did not lead to any damage. SiC + 2%AlN showed the same behaviour under irradiation with identical parameters. Stainless steel reacts highly sensitive to shorter irradiation times of 10 to 30 s at energies of 20 to 30 MeV with grain growth and melts under irradiation with 20 MeV for 60 s. After solidification of the melt the solidified metal shows interdendritical cracks. Molybdenum proves to be less sensitive to 20 to 30 MeV irradiation at times of 45 to 60 s showing grain growth but no melting. An irradiation of tungsten with 30 MeV and 30 s leads to grain growth and microcracking of the surface. A SEM-image of the surface of the tungsten specimen exposed to 30 MeV for 30 s is shown in Figure 2.

Thus, in relative comparison, graphite and SiC+2%AlN show the highest structural resistivity against MeV electron impact.

3.2 Experimental results on layer systems

The work focus on layer systems lies in compound systems of plasma facing low Z and low density materials (e.g. graphite) attached to high Z and high density materials (e.g. stainless steel or molybdenum) by brazing or hot isostatic pressing (HIP).

For screening purposes and simplified post-experimental examination initial experiments on layer systems have been carried out with graphite plates of two, five and ten millimeter thickness fixed mechanically with nuts and bolts to 10 mm stainless steel and molybdenum base plates. Beam incidence was normal to the graphite surface of the specimens. The parameters and results of the experiments on model layer systems are given in Table 4.

Except for some discoloration at longer irradiation times of 45s and 60s the graphite layers did not show damage. A comparison of the results on layer systems with stainless steel substrates and the results on stainless steel bulk specimens does not show significant difference in the damage thresholds for the case of 2 mm and 5 mm thick graphite layers. Only a shielding of 10mm thick graphite reduces the damage on stainless steel substrates compared to unshielded bulk stainless steel.

The model layer systems of molybdenum covered by graphite suffered serious damage (Figure 3). The molybdenum substrates covered by 2 mm and 5mm thick graphite were subjected to high temperature excursions. Molybdenum itself shows only (slight) grain growth, similar to the results on bulk molybdenum. The temperature of the substrate

nevertheless exceeded the melting temperature of stainless steel thus causing melting of the attachment parts. As in the case of graphite/ stainless steel structures, only a graphite layer of 10 mm thickness provides sufficient shielding of the molybdenum substrate to prevent any observable damage.

For further determination of high energy electron impact effects on actively cooled components brazed layer systems have been tested. Figure 4 shows the results of experiments on systems of 5 mm and 10 mm thick graphite brazed to compound substrates composed of a 2 mm molybdenum layer, a 2.5 mm thick copper layer, and a 2 mm thick molybdenum layer. After irradiation of both samples with 20 MeV and 60 s the sample with a 5mm thick graphite layer shows complete melting of the intermediate copper phase. In the location of the brazed zone between the 5 mm graphite layer and molybdenum small droplets are found which may originate from the Cu-Ag-Ti braze used for bonding. The specimen with a graphite layer thickness of 10 mm does not show visible damages. Thus also in the case of brazed layer systems, like in the case of the before mentioned model layer systems, a thickness of 10 mm graphite provides significant shielding compared to graphite layers of 5 mm thickness.

4. Discussion

During the impact of high energy electrons on matter the electron energy is deposited in the volume of the material in contrast to surface energy deposition in lower electron energy cases. The volume deposition process is mainly determined by the electron energy E, the density ρ and the

average atomic number Z_{av}. The physical factors in high energy beam - materials interaction that have to be regarded are the electron range /7/, the electron stopping power /8/, the energy absorption along the range /9,10/, photon production /11/, Compton effect /12/ and pair production processes /13,14/.In a theoretical approach to quantitatively determine the volume energy deposition by high energy electrons Monte Carlo simulation codes have to be applied which consider all of these factors. Fusion technology related Monte Carlo calculations are performed at Sandia National Laboratories, Albuquerque /15/.

For a basic understanding of the experimental results obtained by high energy electron irradiation of materials the electron range, the energy absorption along this range and the critical energy as a parameter for the ratio of radiation to thermal energy deposition have to be regarded.

range:
Above an energy of 1 MeV the average electron range r in a target material can be approximated as follows:

$$r = \frac{1}{\rho}(0.51 \cdot E - 0.26) \qquad \text{/7/ eq. (1)}$$

with ρ introduced in g/cm^3, E in MeV, and r in cm.

absorption of energy in the material:
Along the electron range the deposition of energy in material is not constant. Being almost independent of the beam energy the absorption can be expressed as:

$$\frac{P_A(z)}{P_{A\,max}} = 1 - \frac{9}{4}\left(\frac{z}{r} - \frac{1}{3}\right)^2 \qquad /7/ \text{ eq. (2)}$$

$P_A(z)/P_A max$ is the ratio of power absorbed per unit volume at a distance z from the sample surface to the maximum deposited power in the material depth. This quantity reaches unity (maximum energy deposition) at a distance $z = r/3$. This ratio is almost independent of the electron energy. Thus in the runaway-electron impact case the energy is directly deposited in the volume of the material whereas usual surface heat loads lead to a heating of the material volume by heat transfer processes.

photon production:

With increasing beam energy and with increasing atomic number Z the portion of beam energy expended for photon production due to radiative collisions with atoms increases. The energy E_c (critical energy) where half of the beam power is converted into x-ray (bremsstrahlung) is given as:

$$E_c = 800/(\,Z + 1.2\,) \qquad /13/ \text{ eq. (3)}$$

Table 5 gives the values of range and critical energy derived from equations (1) and (3) for materials tested in the runaway-electron simulation experiments. Thus with regard to the thermal energy deposition the effects of the density ρ, and the atomic number Z are controversial. Low density and low Z_{av} lead to a favourable deposition of the thermal load in large material volumes but the major part of the kinetic energy is converted to thermal energy whereas in the high density and high Z_{av} case the fraction of the thermal energy is less but

the heat load is deposited in far smaller volumes. Thus, with consideration of the physical material properties listed in Table 1 several statements on the experimental results can be made.

Due to the long range of electrons in graphite the thermal energy is deposited in a very large volume leading to moderate temperature excursions of the material. Under high energy electron impact this happens even if most of the kinetic electron energy is transformed into thermal energy compared to minor emission of bremsstrahlung. High thresholds for thermal induced damages like erosion and cracking /16/ lead to superior resistance of graphite materials against runaway-electron impact in the energy range of 20 to 30 MeV.

The moderate density of SiC leads to an uncritical energy distribution in the bulk much like that in graphite. The heating rate in the material volume obviously stays below the limit of thermal shock damage occurance in the experiments described in this paper.

Stainless steel reacts sensitive to high energy electron impact with grain growth and melting. Because of the high density of the material the energy deposition happens in rather small material volumes. Additionally poor thermal conductivity, a low threshold for twin formation and grain growth ($T > 0.7\ T_M$), as well as a low melting point lead to severe damage under high energy electron impact.

The molybdenum samples in the experiments underwent high thermal loads due to unfavourable distribution of the beam energy in small material volumes caused by the high density of molybdenum. The thermal induced

damages in molybdenum were far less severe compared to stainless steel due to the high melting point and thus also a high threshold for grain growth initiation in molybdenum.

Although in the high Z material tungsten the major part of the beam energy is expended into bremsstrahlung production tungsten seems to undergo extensive temperature excursions due to the extremely short range of electrons which causes energy deposition in very small volumes. In addition part of the bremsstrahlung photons also contribute to the thermal loads by pair production processes. Thus under high energy electron impact on tungsten the temperature threshold for grain growth is easily exceeded. The coarse grain structure developing under these conditions is highly prone to microcracking when the ductile-brittle transformation temperature (DBTT) is passed during the cooling phase after the electron impact.

In layer systems of graphite covering metal substrates most of the kinetic energy of the electrons is deposited in the metal unless very thick graphite shielding is provided. This is caused by the long range of high energy electrons in graphite. Thus in the case of 2mm and 5mm graphite layers only a neglegible fraction of the beam energy is deposited in the graphite layer whereas a layer of 10 mm graphite absorbs a portion of the beam energy to provide some reduction of the thermal load imposed on the substrate material. Like the results on bulk materials stainless steel substrates are more sensitive to high energy electron impact than molybdenum substrates. Also in compound systems special attention has to be paid to the brazed interface. Braze materials with a comparatively low melting point such as copper base brazes may be subjected to melting and structural changes.

5. Conclusions

The following conclusions on first wall bulk materials can be drawn:

In the experiments graphite and SiC showed the highest resistance against 20 to 30 MeV electron impact. Among metals stainless steel suffered severe damage like grain growth and melting. Molybdenum heats up to high temperatures but only shows minor damage. Tungsten undergoes grain growth and microcracking under 20 to 30 MeV electron impact.

Additionally experiments were performed on layer systems consisting of graphite layers on metal substrates which resemble the structure of actively cooled systems. The preliminary results indicate that molybdenum cooling tubes are preferable to stainless steel and presumably also to copper cooling tubes due to the higher thermal damage threshold of molybdenum. For brazing materials a braze with a high melting point (e.g. Zr-braze) is preferable. Thick graphite volumes covering cooling tubes should be chosen to minimize heat loads by direct electron heating of the coolant tubes.

References

/1/ Dreicer, H., Phys. Rev., 115,2 (1959) 238

/2/ Lomer, W. M., J. Nucl. Mater. 133&134 (1985) 18

/3/ Nishikawa, M., Yokomizo, H., Kitsunezaki, A., Mc Kelvey, T. E., Taylor, T. S., Doll, D., Brook, N., Seraydarian, R., J. Nucl. Mater. 128&129 (1984) 493

/4/ Dietz, K. H. in: Proc. of the Japan - US Workshop on Plasma Material Interaction / High Heat Flux Data Needs for the Next Step Ignition and Steady State Devices, Institute of Plasma Physics, Nagoya University, Jan. 26 - 30, 1987, IPPJ-AM-50

/5/ Kotzlowski, H. E. in: Proc. 13th Symp. on Fusion Technology (1984) 1253

/6/ Koizlik, K., Bolt, H., Hoven, H., Linke, J., Nickel, H., Wallura, E., in: 14th Symp. on Fusion Technology, Avignon (1986), to be published

/7/ Schiller, S., Heisig, U., Panzer, S., Electron Beam Technology, (John Wiley & Sons, New York, 1982)

/8/ Pal, P. B., Varshney, V. B., Gupta, D. K., Nucl. Instr. Meth. B16 (1986) 1

/9/ Birkhoff, R. D., in: S. Fluegge ed., Handbuch der Physik, Vol.34, (Springer, Berlin, 1955), pp.121-138

/10/ Tabata, T., Ito, R., Nucl. Sci. Eng. 53 (1974) 226

/11/ Koch, H. W., Motz, J. W., Rev. Mod. Phys., 31,4 (1959) 920

/12/ Evans, R. D., in: Fluegge, S., ed., Handbuch der Physik, Vol.34, (Springer, Berlin, 1955), pp. 219-298

/13/ Swanson, W. P., Radiological Safety Aspects of the Operation of Electron Linear Accelerators, IAEA Technical Report Series No. 188, (IAEA, Vienna, 1979)

/14/ Alsmiller, R. G., Moran, H. S., Nucl. Instr. Meth. 48 (1967) 109

/15/ Whitley, J. B., Koski, J. A., Aymar, R. in: 14th Symp. on Fusion Technology, Avignon (1986), to be published

/16/ Bohdansky, J., Croessmannn, C. D., Linke, J. in: 14th Symp. on Fusion Technology, Avignon (1986), to be published

Captions of Tables

Table 1: Runaway-electron simulation parameters

Table 2: Bulk materials used in electron linear accelerator experiments, specimen size and relevant physical properties

Table 3: Damage thresholds of bulk materials

Table 4: Results of linear accelerator experiments on layer systems

Table 5: Electron range and critical energy of tested materials

Figure captions

Figure 1: Set-up for linear accelerator experiments. The electron beam is coupled into the target chamber via 20 µm thick Ti-foils. Beam incidence onto the specimen surface is perpendicular.

Figure 2: Surface of tungsten specimen after electron irradiation with 30 MeV for 30 s. The irradiation caused grain growth and microcracking (SEM micrograph)

Figure 3: Model layer systems after electron irradiation with 20 MeV for 45s. Graphite layers (left) have been attached to molybdenum substrates (right) by stainless steel nuts and bolts. Thermal excursions of the substrates in the case of thin graphite layers caused melting of the attachment parts.

Figure 4: Brazed layer systems of graphite brazed to Mo-Cu-Mo substrate after electron irradiation with 20 MeV for 60 s. The specimen with a graphite layer of 5 mm thickness (left) underwent melting of the Cu-phase and degradation of the braze zone between graphite and Mo. The specimen with a 10 mm graphite layer (right) shows no damage.

beam energies and	
beam pulse currents:	E = 20 MeV, I_p = 300 mA
	E = 25 MeV, I_p = 280 mA
	E = 30 MeV, I_p = 240 mA
pulse width	: t_p = 1.5 μs
repetition rate	: f = 120 pps (pulses per sec.)
input power	: P = 1.06 kW (20 MeV)...1.30kW (30 MeV)
beam diameter	: d = 4 mm
irradiation times	: t_{irr} = 10...60 s

Table 1: Runaway-electron simulation parameters

material	graphite	SiC+2%AlN	stainl. steel	Mo	W
supplier/ country	Ringsdff. FRG	Hitachi Japan	Novonox FRG	Metallwerk Plansee Austria	
trade name	EK 98	Hitaceram	SS 316, 1.4311		
specimen geometry (mm)	15x15x30	10x10x25	dia.20x30 dia.20x10	dia.20x30 dia.20x10	dia.20x30 dia.20x10
density (g/cm^3)	1.8	3.2	8.0	10.2	19.3
average atomic no. (Z, Z_{eff})	6	10	25.7	42	74
melting point (^oC)		(2425)	1450	2615	3405
thermal conductivity (W/cmK) at RT	0.6	1.0	0.15	1.38	1.74
spec. heat (J/gK) at RT	0.75	0.75	0.5	0.25	0.13

Table 2: Bulk materials used in electron linear accelerator experiments, specimen size and relevant physical properties

material	no damages occured	threshold ($E;t_{irr}$) for slight grain growth	threshold ($E;t_{irr}$) for grain growth	melting	cracking
graphite (EK 98)	20...30MeV 60s				
SiC+2%AlN	20...30MeV 60s				
st. steel (1.4311)		20...30MeV 10s	20...30MeV 30s	20MeV 60s	20MeV 60s (interdendr.)
Mo		20MeV 45s	20...30MeV 60s		
W			30MeV 30s		30MeV 30s

Table 3: Damage thresholds of bulk materials

system	energy and irrad. time	observed damages
2mm graphite + 10mm st. steel	30MeV, 10s	twin formation /6/ on substrate
5mm graphite + 10mm st. steel	30MeV, 10s	initial twin formation on substrate
10mm graphite+ 10mm st. steel	30MeV, 10s	---
5mm graphite + 10mm st. steel	20MeV, 60s	initial melting of st. steel substrate
10mm graphite+ 10mm st. steel	20MeV, 60s	grain growth on substrate
2mm graphite + 10mm Mo (TZM)	20MeV, 45s	melting of stainless steel attachment bolts, grain growth on substr. (fig. 3)
5mm graphite + 10mm Mo (TZM)	20MeV, 45s	initial melting of attachment bolts, slight grain growth on substrate (fig.3)
10mm graphite+ 10mm Mo (TZM)	20MeV, 45s	--- (fig.3)

Table 4: Results of linear accelerator experiments on layer systems

material	range (mm) at		critical energy E_c (MeV)
	20MeV	30MeV	
graphite	55.2	83.6	111.1
SiC + 2%AlN	31.1	47.0	62.5
st. steel	12.4	18.8	29.4
Mo	9.7	14.7	18.5
W	5.2	7.8	10.6

Table 5: Electron range and critical energy of tested materials

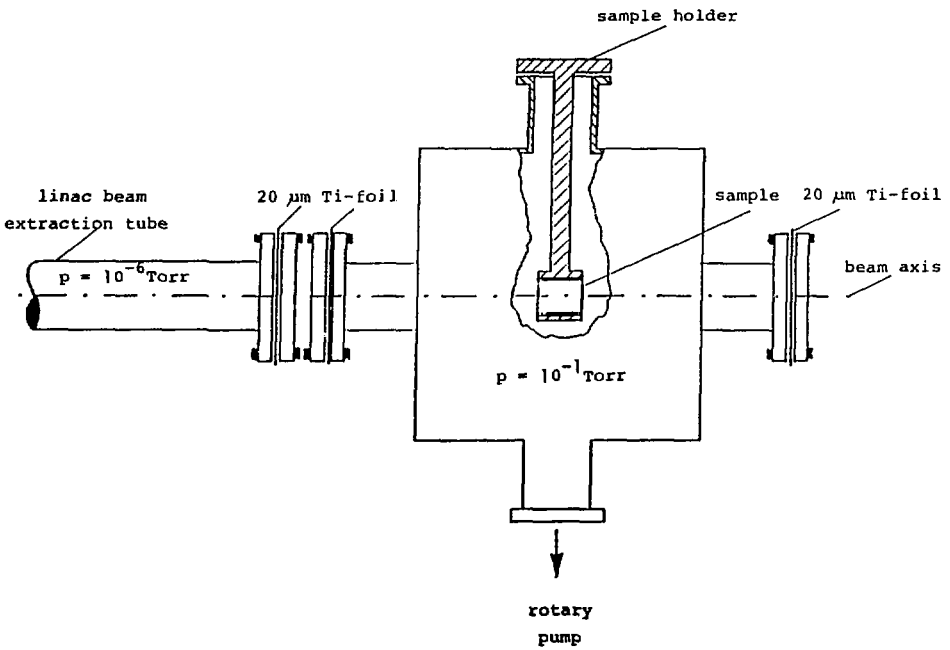

Figure 1: Set-up for linear accelerator experiments. The electron beam is coupled into the target chamber via 20 µm thick Ti-foils. Beam incidence onto the specimen surface is perpendicular.

Figure 2: Surface of tungsten specimen after electron irradiation with 30 MeV for 30 s. The irradiation caused grain growth and microcracking (SEM micrograph)

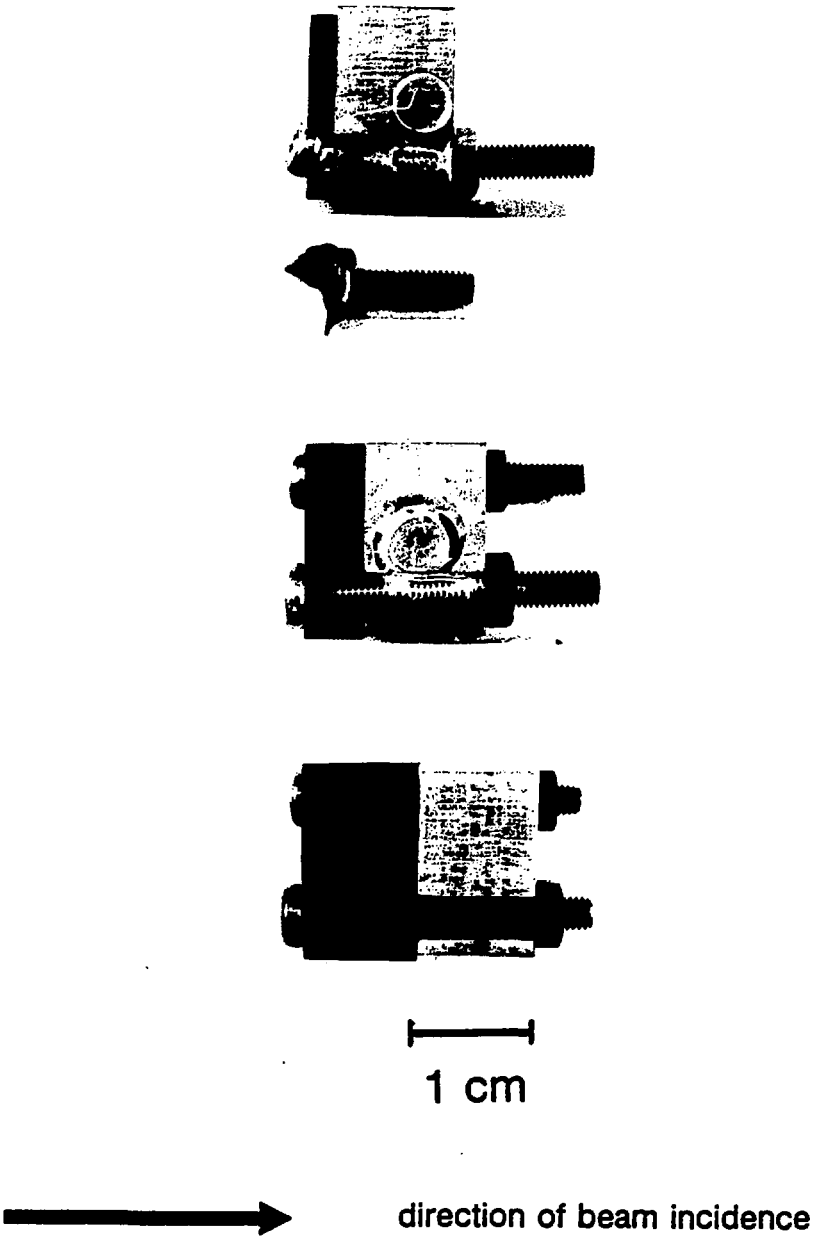

Figure 3: Model layer systems after electron irradiation with 20 MeV for 45s. Graphite layers (left) have been attached to molybdenum substrates (right) by stainless steel nuts and bolts. Thermal excursions of the substrates in the case of thin graphite layers caused melting of the attachment parts.

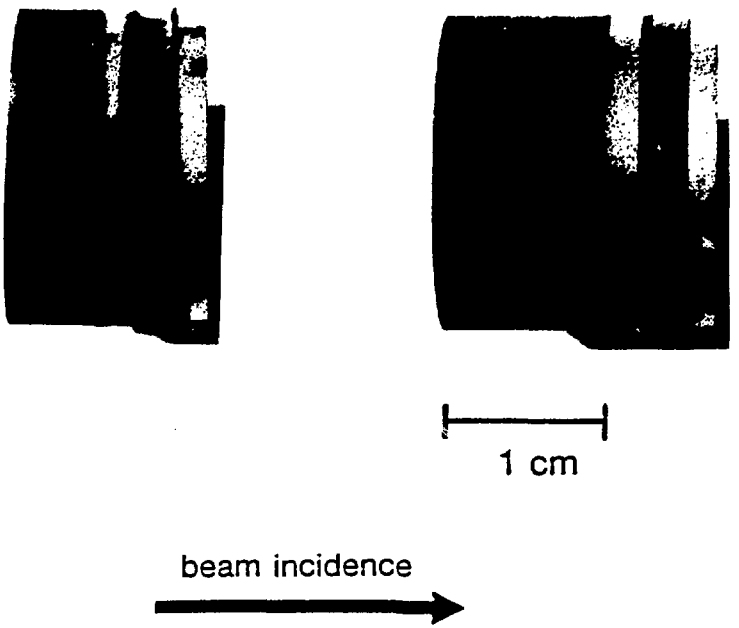

Figure 4: Brazed layer systems of graphite brazed to Mo-Cu-Mo substrate after electron irradiation with 20 MeV for 60 s. The specimen with a graphite layer of 5 mm thickness (left) underwent melting of the Cu-phase and degradation of the braze zone between graphite and Mo. The specimen with a 10 mm graphite layer (right) shows no damage.